Rotation–vibration energy cluster formation in XH_2D and XHD_2 molecules (X = Bi, P, and Sb)

Sergei N. Yurchenko [a], Roman I. Ovsyannikov [b,1], Walter Thiel [c], Per Jensen [b,*]

[a] Technische Universität Dresden, Institut für Physikalische Chemie und Elektrochemie, D-01062 Dresden, Germany
[b] Theoretische Chemie, Bergische Universität, D-42097 Wuppertal, Germany
[c] Max-Planck-Institut für Kohlenforschung, Kaiser-Wilhelm-Platz 1, D–45470 Mülheim an der Ruhr, Germany

ARTICLE INFO

ABSTRACT

We investigate theoretically the energy cluster formation in highly excited rotational states of several pyramidal XH_2D and XHD_2 molecules (X = Bi, P, and Sb) by calculating, in a variational approach, the rotational energy levels in the vibrational ground states of these species for $J \leqslant 70$. We show that at high J the calculated energy levels of the di-deuterated species XHD_2 exhibit distinct fourfold cluster patterns highly similar to those observed for H_2X molecules. We conclude from eigenfunction analysis that in the energy cluster states, the XHD_2 molecule rotates about a so-called localization axis which is approximately parallel to one of the X–D bonds. For the mono-deuterated XH_2D isotopologues, the rotational spectra are found to have a simple rigid-rotor structure with twofold clusters.

© 2009 Elsevier Inc. All rights reserved.

1. Introduction

The formation of rotation–vibration energy clusters at high rotational excitation has been theoretically predicted for H_2O, H_2S, H_2Se, H_2Te, CH_4, CF_4, SiH_4, SbH_4, SF_6, PH_3, BiH_3, and SbH_3 by semiclassical methods and in quantum-mechanical, variational calculations of rotation–vibration energy levels [1–22]. The energy clusters have been experimentally observed for H_2Se [13,23,24], CH_4, SiH_4 (see [10] and references therein), and SF_6 [25].

We have already employed the program XY3 [26], which computes the rotation–vibration energies of an XY_3 pyramidal molecule in an isolated electronic state variationally, to study the energy cluster formation in PH_3 [20,21], BiH_3, and SbH_3 [22] by calculating ro-vibrational energies at extremely high values of the angular momentum quantum number J. The XY3 approach has been developed for simulating the rotation–vibration spectra of pyramidal XY_3 molecules [26,27] and is based on the Hougen–Bunker–Johns (HBJ) formalism [28], where the vibrational motion is viewed as producing displacements from a flexible reference configuration defined by Eckart–Sayvetz conditions [29,30]. Apart from the qualitative studies of energy cluster formation reported in Refs. [20–22], we have utilized the XY3 approach to make quantitatively accurate intensity simulations at moderate rotational excitation ($J \leqslant 20$) for several XY_3 molecules [21,27,31,32]. XH_3 molecules exhibit sixfold energy clusters [20,22], different from the fourfold clusters found in H_2X molecules [33]. In the H_2X case, the energy level pattern is such that at a particular critical J-value J_c, the fourfold energy cluster formation sets in [14,17,34], whereas for XH_3 molecules, the clusters form more gradually and no critical J-value can be defined [20,22,35].

The formation of energy clusters takes place at very high rotational excitation and so it can be satisfactorily described both by quantum-mechanical and classical approaches. It adds a highly interesting dimension to the study of the energy clusters that the complex quantum processes leading to the cluster formation can be analyzed and explained in terms of classical theory, that is, theory in accordance with everyday experience.

In the quantum study of the cluster formation it is customary to introduce so-called *primitive cluster states* (PCSs) [14,19,20]. In the classical description [1,3,36], PCSs correlate with stable rotations about so-called *localization axes*. For H_2X and XH_3 molecules, a

---

localization axis approximately coincides with one of the equivalent X–H bonds in the molecule [17]. An analysis of the topology of the classical or semi-classical *rotational energy surface* (RES) [17,20,22,35,37–41], in particular of the stationary points on the RES, determines these localization axes and predicts the critical angular momentum value J_c for H_2X molecules [14,17,34].

Very recently we have developed a new theoretical model for the rotation and vibration of molecules with associated computer program TROVE [42] (Theoretical ROtation–Vibration Energies). TROVE is an extension of the XY3 program and applicable to the calculation of rotation–vibration energies of arbitrary polyatomic molecules in isolated electronic states. Just like XY3 calculations, TROVE calculations are variational and have the nuclear kinetic energy operator represented as a series expansion in terms of vibrational coordinates. Whereas with XY3, we were limited to calculate rotation–vibration energies of XH_3 molecules, with TROVE we can extend the calculations to the deuterated species XH_2D and XHD_2 (X = Bi, P, and Sb). In the present work, we investigate the (possible) energy cluster formation in these molecules by calculating the rotation–vibration energy levels for $J \leqslant 70$.

In previous theoretical, quantum-mechanical studies of the fourfold energy cluster formation in H_2X molecules (see Refs. [19,33] and references therein), it was generally found that the corresponding deuterated species HDX had no energy clusters due to lack of symmetry. The di-deuterated species D_2X were assumed to exhibit energy clusters but at J values so high that the corresponding energies could not be practically calculated. In the present study, we investigate whether energy clusters are formed in the deuterated molecules XH_2D and XHD_2. In order that a near-degenerate, N-fold energy cluster can form, certain requirements must be met: The molecule in question must have $N/2$ equivalent X–Y bonds, connecting a heavy central atom X with a much lighter Y atom. The bonds must be nearly orthogonal to each other and there must be little coupling between the associated stretching modes. Although each of the pyramidal molecules XH_2D and XHD_2 has two equivalent bonds, the existence of a stable rotation axis at high J is not immediately obvious. We find here that in the case of XHD_2 molecules, fourfold energy clusters form at high J, whereas for XH_2D molecules, only the twofold clusters known from rigid-rotor theory are formed.

In the present work, we use both quantum and classical approaches to analyze the rotational dynamics of the molecules under investigation. We solve, on one hand, the Schrödinger equation and, on the other hand, we generate RESs from the classical analogue of the quantum-mechanical Hamiltonian. With the technique described in Ref. [14] we determine the directions of the (classical) localization axes from the (quantum-mechanical) TROVE eigenfunctions by maximizing the expectation values of the angular momentum projections. We also reconstruct the (classical) RES by using information extracted from the (quantum-mechanical) eigenfunctions in a so-called 'semi-quantum' analysis [22].

Due to the very pronounced local-mode behaviour of BiH_3 and SbH_3 [19,43,44], we have found previously [22] that energy clusters form at lower J values in these molecules than in PH_3 [20,21]. Besides BiH_3 is an almost perfect, accidental spherical top [45] and therefore its energy clusters form more readily than those of SbH_3 [22]. This makes BiH_3 an ideal object for studying different aspects of the cluster formation since the clusters form at the lowest possible J values for which the energies can be calculated at the lowest computational cost. Consequently, in the present work we make the most detailed analyses for $BiHD_2$ and BiH_2D.

The paper is structured as follows. In Section 2, we describe the variational method used to solve the rovibrational Schrödinger equation, present the theoretical rotational term values of the XH_2D and XHD_2 (X = Bi, P, and Sb) molecules in their ground electronic states, and discuss the formation of the rotational energy clusters. The primitive cluster states and their analysis are presented in Section 3. In Section 4, we offer a classical explanation of the rotational clusters by means of the rotational energy surfaces and the 'semi-quantum' analysis [22]. The prospects of an experimental observation of the energy clusters are discussed in Section 5. Section 6 presents conclusions.

2. Variational method

As mentioned above, we employ the variational program TROVE [42] for the nuclear-motion calculations of the present work. The TROVE theoretical model and the accompanying computer program are designed for computing the ro-vibrational energies for polyatomic molecules of general structure. A basic feature of the model is the use of expansions in linearized vibrational coordinates to represent both the kinetic energy operator and the potential energy function. In order to characterize the rotation–vibration energy clusters it is necessary to be able to calculate rotational energies for very high J, typically $J \leqslant 70$. It has been shown in Refs. [20,22] that even with a relatively small vibrational basis set, the energy clusters can be described qualitatively in XH_3 molecules for J up to 70.

In the TROVE approach, the vibrational basis functions [42] are given by:

$$\phi_n = |n_1\rangle |n_2\rangle |n_3\rangle |n_4\rangle |n_5\rangle |n_6\rangle, \tag{1}$$

where $|n_i\rangle$ (with n_i as the principal quantum number) is a one-dimensional (1D) function $\phi_{n_i}(\xi_i^\ell)$ depending on one, and only one, of the six coordinates ξ_i^ℓ ($i = 1 \ldots 6$) which are linearized versions [26] of the coordinates $(r_1, r_2, r_3, \alpha_{12}, \alpha_{13}, \alpha_{23})$ for the XH_3 molecule. Here, r_i is the instantaneous value of the distance between the central X nucleus and H_i, the proton labeled $i = 1, 2$, or 3. The bond angle $\alpha_{jk} = \angle(H_j X H_k)$. The $\phi_{n_i}(\xi_i^\ell)$ functions are generated as numerical solutions of the corresponding 1D Schrödinger equations (for details, see Ref. [42]). In the present TROVE calculations, we use a Hamiltonian defined in terms of a rigid reference configuration, i.e., both the kinetic energy operator and the potential energy function are expressed as expansions (of 4th and 8th order, respectively) around the equilibrium geometry in the coordinates ξ_i^ℓ ($i = 1 \ldots 6$).

We follow Refs. [20,22,42] in defining the vibrational basis set in terms of the polyad number

$$P = 2(n_1 + n_2 + n_3) + n_4 + n_5 + n_6. \tag{2}$$

We include in the basis set only those basis functions ϕ_n for which $P \leqslant P_{\max}$. In the present work we take, as in Ref. [20], the vibrational basis set to consist of all basis functions with $P \leqslant 6$.

In order to facilitate the construction of the Hamiltonian matrix at high J, and improve the convergence with increasing basis set, we optimize the ro-vibrational basis functions in a contraction scheme as follows. For $J = 0$, the vibrational Hamiltonian is diagonalized in a basis of functions ϕ_n from Eq. (1). The resulting vibrational ($J = 0$) eigenfunctions ϕ_v^{vib} are combined with rigid-rotor functions $|J, k, m\rangle$ (see, for example, Ref. [46]) to form the contracted basis functions for the $J > 0$ eigenstates:

$$\phi_{v,k}^{J,m} = |J, k, m\rangle \phi_v^{\text{vib}}. \tag{3}$$

The molecule-fixed axis systems chosen for the XH_2D and XHD_2 molecules (Fig. 1) are principal axes at equilibrium and we label them as *abc* [46] in the figure. In defining the rigid-rotor functions $|J, k, m\rangle$ [46] we make the identifications $xyz = abc$ for XH_2D and $xyz = cab$ for XHD_2. The XH_2D molecules are near-prolate asymmetric tops at equilibrium. For example, BiH_2D has the equilibrium rotational constants $A_e = 2.66$ cm^{-1}, $B_e = 1.78$ cm^{-1}, and $C_e = 1.77$ cm^{-1}. On the other hand, the XHD_2 molecules are near-oblate asymmetric tops. $BiHD_2$ has the equilibrium rotational constants $A_e = 1.79$ cm^{-1}, $B_e = 1.77$ cm^{-1}, and $C_e = 1.34$ cm^{-1}.
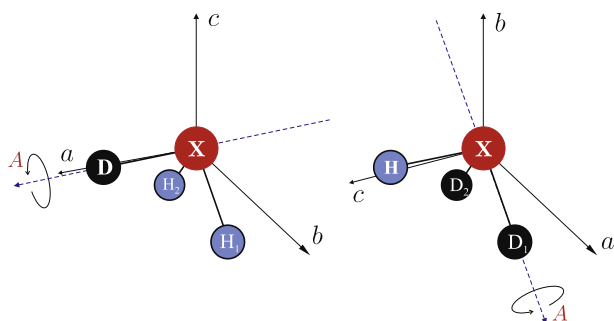
Fig. 1. The labeling of the nuclei chosen for XH_2D and XHD_2, the principal axes *abc*, and a localization axis *A* (see text).

The use of the new basis functions $\phi_{v,k}^{J,m}$ in Eq. (3) simplifies substantially the calculation of the Hamiltonian matrix elements. In particular, the vibrational part of the Hamiltonian is diagonal in this basis; the diagonal matrix elements are the $J = 0$ energies which are known from the $J = 0$ calculation so that they do not have to be computed. All necessary vibrational integrals of the rotational and Coriolis parts of the kinetic energy operator are pre-computed using the $J = 0$ eigenfunctions and stored on disk. More details of this part of the calculation will be given elsewhere.

The potential energy functions for the electronic ground states of BiH_3, PH_3, and SbH_3 that we use in the present work are taken from Refs. [22,31]. The results of the TROVE calculations for BiH_2D, $BiHD_2$, PH_2D, PHD_2, SbH_2D, and $SbHD_2$ are collected in Figs. 2–4. The figures are presented as *cluster formation diagrams* in that we plot the term value spacings $E_{v=0J,K} - E_{v=0J,K}^{max}$ where E_{Jk} is the term value of the level characterized by the quantum numbers J, k (see, for example, [46]) and $E_{v=0J,K}^{max}$ is the maximum energy of the J multiplet in question.

We see in the bottom displays of Figs. 2–4 that for the mono-deuterated species XH_2D, only twofold energy clusters form in the range of J values considered. These are the usual doubly degenerate states typical for asymmetric tops and associated with the fact that the states with $k = \pm|k|$ become degenerate for high J and $|k| [19,47]$. The top displays of Figs. 2–4, however, show that the di-deuterated species XHD_2 have energy level patterns distinctly different from those of the XH_2D molecules: The di-deuterated species exhibit fourfold cluster patterns highly similar to those observed for H_2X molecules (see, for example, Fig. 1 of Ref. [18]). Owing to the lack of energy clusters, the XH_2D species are of little further interest in the present study and we focus on the XHD_2 molecules.

Comparison of the top displays in Figs. 2–4 confirms that as already suggested above, relative to PHD_2 and $SbHD_2$ the fourfold clusters form at lower J-values in $BiHD_2$. In Fig. 5, the left-hand display shows the top part of the cluster formation diagram for $BiHD_2$. If we number the energies in a given J manifold as $E_1, E_2, E_3, E_4 \ldots$, in order of decreasing energy (so that $E_1 = E_J^{max}$), the difference $E_1 - E_4 > 0$ is the *cluster spread* for the top cluster. The cluster spreads for the vibrational ground state of $BiHD_2$ are plotted against J in the right-hand display of Fig. 5. At low J, it increases with J until it reaches a maximum at the critical J-value $J_c(= 20$ here). At $J > J_c$ it decreases very rapidly with J. The variation of the cluster spread with J that we find for the vibrational ground state of $BiHD_2$ is also found for the vibrational ground states of several H_2X molecules, chiefly H_2S, H_2Se, H_2Te, and H_2Po (see Ref. [33] and the references therein). Classically, the variation of the cluster spread with J for an H_2X molecule can be considered as the result of a 'bifurcation process' [17]: As J increases, the axes with the smallest moments of inertia lose their stability and the molecule starts rotating about new stable axes that, in the case of H_2X molecules,
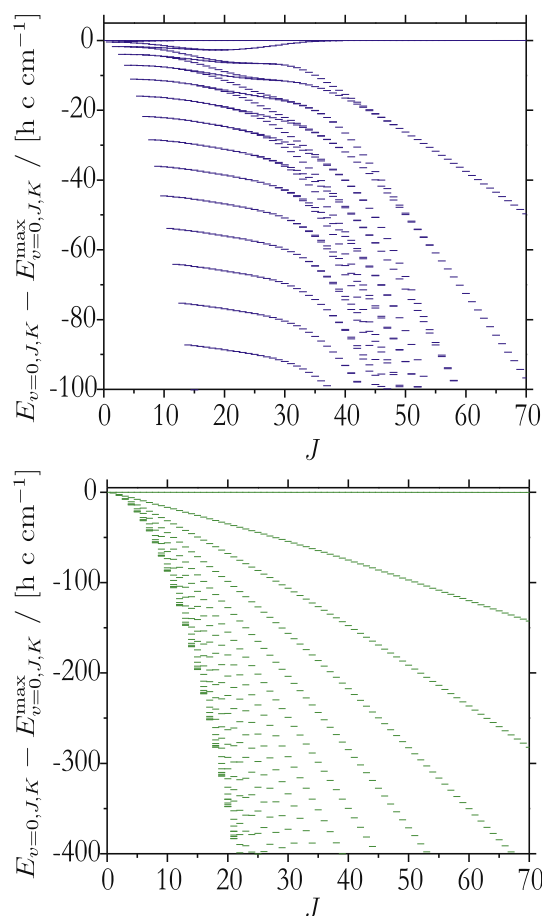

Fig. 2. The calculated rotational energy structure in the vibrational ground state of $BiHD_2$ (top) and BiH_2D (bottom). Term values $E_{v=0J,k}$ are plotted relative to the highest term $E_{J,k}^{max}$ for each J multiplet.

approach the X–H bonds at high J values. From Figs. 3 and 4, we obtain values of $J_c = 38$ and 27 for PHD_2 and $SbHD_2$, respectively.

3. Analysis of the primitive cluster states

3.1. Symmetry

The variationally obtained rotation–vibration wavefunctions $\psi_n^{J,\Gamma}$ are linear combinations of basis functions $\phi_{v,k}^{J,m}$:

$$\psi_n^{J,\Gamma}(r_1, r_2, r_3, \alpha_{12}, \alpha_{13}, \alpha_{23}, \theta, \phi, \chi) = \sum_{k=-J}^{J} \sum_v C_{v,k}^{n,J,\Gamma} \phi_{v,k}^{J,m}, \qquad (4)$$

where the $C_{v,k}^{n,J,\Gamma}$ are expansion coefficients, Γ is the $\mathbf{C}_s(M)$ symmetry of the wavefunction $\psi_n^{J,\Gamma}$, n is an index distinguishing eigenfunctions with the same value of Γ. We label the energies determined in the variational calculation by the k-value k_{lc} (where the subscript letters 'lc' stand for 'largest contribution') of the basis function $\phi_{v,k}^{J,m}$ with the largest contribution to the eigenfunction $\psi_n^{J,\Gamma}$, i.e., with the largest value of $|C_{v,k}^{n,J,\Gamma}|^2$. For low J we find $k_{lc} = k$, where k is the angular momentum projection value expected from rigid-rotor theory. We generally denote by ψ_i^{Γ}, $i = 1, 2, 3, 4$, the wavefunctions $\psi_n^{J,\Gamma}$ belonging to a particular top cluster with a given J value. Here, Γ is the $\mathbf{C}_s(M)$ symmetry of the wavefunction in question. The molecular symmetry (MS) Group $\mathbf{C}_s(M) = \{E, (12)^*\}$ [46], where E is the identity operation and $(12)^*$ is the interchange of the two D nuclei combined with the spatial inversion operation E^* [46]. The irreducible representations of $\mathbf{C}_s(M)$ are the totally symmetric
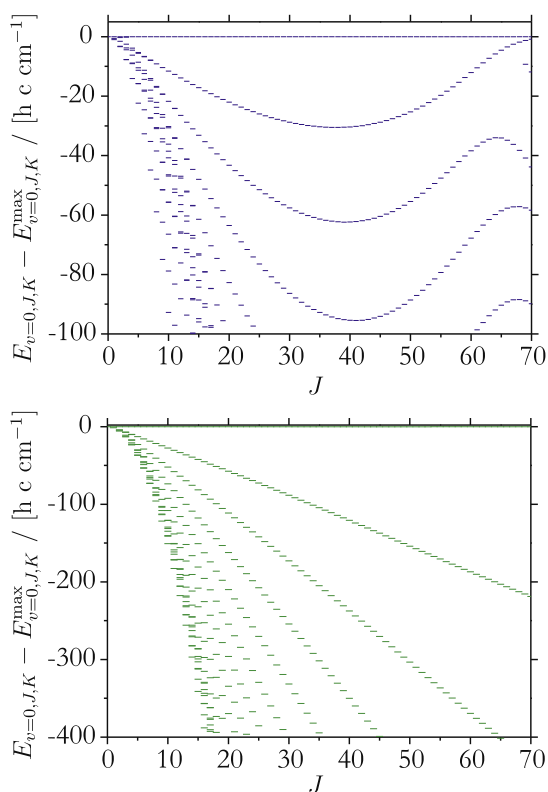
Fig. 3. The calculated rotational energy structure in the vibrational ground state of PHD$_2$ (top) and PH$_2$D (bottom). Term values $E_{v=0,J,k}$ are plotted relative to the highest term $E_{v=0,J,k}^{max}$ for each J multiplet.
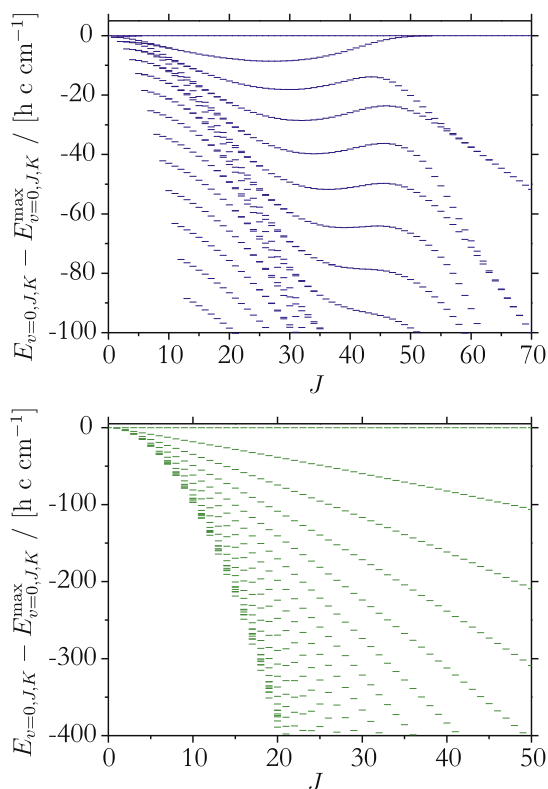

Fig. 4. The calculated rotational energy structure in the vibrational ground state of SbHD$_2$ (top) and SbH$_2$D (bottom). Term values $E_{v=0,J,k}$ are plotted relative to the highest term $E_{J,k}^{max}$ for each J multiplet.

representation A' together with the representation A'' which describes a sign change under $(12)^*$ [46].

For a given value of J, the highest four energy levels of an asymmetric rotor such as BiHD$_2$, taken in descending order, are labeled by $J_{K_a,K_c} = J_{J,0}, J_{J,1}, J_{J-1,1}, J_{J-1,2}$. These four states are found to have the $\mathbf{C}_s(M)$ symmetries A', A', A'', A'' in order of descending energy for J even, and A'', A'', A', A' for J odd.

We have already pointed out that the energy cluster formation in the XHD$_2$ species considered here shows great similarity to that in H$_2$X molecules [33]. Therefore, we can base our analysis of the XHD$_2$ cluster effects on experience from the H$_2$X molecules.

The analysis of the H$_2$X energy clusters was carried out in terms of the primitive cluster states mentioned above (see Ref. [33] and the references therein). In a primitive cluster state $|j\,\text{PCS}\rangle$, $j = 1, 2, 3, 4$, the molecule can be viewed as rotating about a localization axis in a clockwise or anti-clockwise sense [14,15,17]. Owing to the similarity of the energy level patterns, we expect to find analogous effects for XHD$_2$ molecules.

For H$_2$X (see Ref. [33] and the references therein) and XH$_3$ [20] molecules we have introduced the primitive cluster states by first assuming that one such state $|1\,\text{PCS}\rangle$ exists (in this state, the molecule is typically assumed to rotate about the X-(Proton 1) bond in such a way that an observer on Proton 1 would see the rest of the molecule rotate clockwise). We then introduce the remaining $|j\,\text{PCS}\rangle$ by letting the non-trivial symmetry operations in the MS group act on $|1\,\text{PCS}\rangle$. For an H$_2$X molecule, the MS group is $\mathbf{C}_{2v}(M) = \{E, (12), E^*, (12)^*\}$ [46], where (12) is an interchange of the two protons and E^* is the spatial inversion operation. There are three non-trivial operations in $\mathbf{C}_{2v}(M)$ and by letting them act on $|1\,\text{PCS}\rangle$ we obtain three additional PCS states so that we have a total of four PCS states corresponding to the fourfold energy clusters in H$_2$X molecules. In the MS group of the XH$_3$ molecules for which we have studied the energy cluster formation, $\mathbf{C}_{3v}(M)$ [46], there are five non-trivial operations and we obtain a total of six PCS states corresponding to the sixfold clusters. For the XHD$_2$ molecules studied in the present work, there is only one non-trivial operation in the MS group $\mathbf{C}_s(M)$, and we cannot follow exactly the same procedure that we used previously. We can, however, choose to label the quantum states in the CNPI (complete nuclear permutation inversion) group [46], consisting of all possible permutation-inversion operations for the molecule in question. For an XHD$_2$ molecule, the CNPI group is $\mathbf{C}_{2v}(M)$. In $\mathbf{C}_{2v}(M)$, the four states in the top cluster in the vibrational ground state of an XHD$_2$ molecule span the representation $A_1 \oplus B_2 \oplus A_2 \oplus B_1$ [see Table A-5 of Ref. [46] for the irreducible representations of $\mathbf{C}_{2v}(M)$]. The three PCS functions $|j\,\text{PCS}\rangle$, $(j = 2, 3, 4)$ are now generated from $|1\,\text{PCS}\rangle$ as follows: $|2\,\text{PCS}\rangle = (12)\,|1\,\text{PCS}\rangle$, $|3\,\text{PCS}\rangle = E^*\,|1\,\text{PCS}\rangle$, and $|4\,\text{PCS}\rangle = (12)^*\,|1\,\text{PCS}\rangle$.

It should be noted that the operations (12) and E^* are omitted from the MS group $\mathbf{C}_s(M)$ for an XHD$_2$ molecule because they are deemed *unfeasible* [46] in that they convert the molecule between two equivalent minima on its potential energy surface, while these minima are known to be separated by an insuperable energy barrier. The fact that we have to describe the PCS states in $\mathbf{C}_{2v}(M)$ suggests that the formation of fourfold clusters in XHD$_2$ molecules is associated with the existence of the two equivalent minima on the potential energy surface. This constitutes a difference to the H$_2$X molecules whose potential energy surfaces have one minimum only.

It has already been discussed for H$_2$X molecules in Ref. [33] how we can obtain the primitive cluster states as linear combinations of the symmetrized cluster functions:

$$|j\,\text{PCS}\rangle = \sum_{i,\Gamma} C_{i,\Gamma}^{(j)}\,\psi_i^\Gamma. \tag{5}$$

We first construct symmetrized linear combinations of the $|j\,\text{PCS}\rangle$ according to the general techniques of Ref. [46], identify the result-
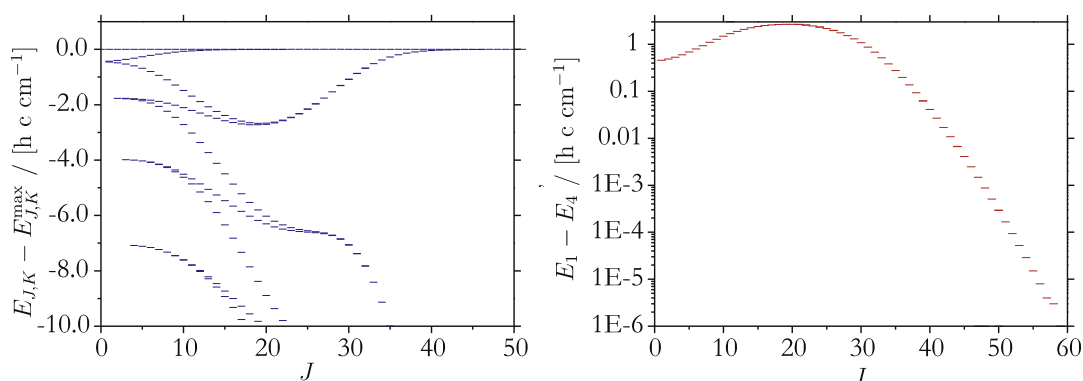
Fig. 5. (Left) The calculated rotational energy structure in the vibrational ground state of BiHD$_2$. Term values $E_{J,k}$ are plotted relative to the highest term $E_{J,k}^{\max}$ for each J multiplet. (Right) The cluster spread (see text) for the top cluster in the vibrational ground state of BiHD$_2$ plotted as a function of J.

ing wavefunctions with the ψ_i^{Γ} functions, and then invert the transformations to obtain Eq. (5).

3.2. The quantum-mechanical definition of the localization axes

We have assumed above that we can introduce four primitive cluster states $|j\,\mathrm{PCS}\rangle$, $j = 1, 2, 3, 4$, for the BiHD$_2$ molecule. Each of these quantum states correlates with a classical situation where the molecule carries out a stable, localized rotation about one of the two equivalent bonds X–D$_1$ and X–D$_2$ in a clockwise or anti-clockwise manner. In order to demonstrate that this is indeed borne out by the TROVE calculations of the present work, we locate the localization axes by a method analogous to that used for H$_2$X molecules in Ref. [15]. The rotation of the H$_2$X molecules was described by means of a molecule-fixed axis system xyz where the y and z axes are defined to be in the molecular plane so that the x axis is perpendicular to this plane. The primitive cluster wavefunction $|j\,\mathrm{PCS}\rangle$ is now rotated about the x axis until the rotated function produces a projection of the angular momentum on the z axis of $-J\hbar$ or $+J\hbar$ [15]. If this is achieved after a rotation about the x axis by an angle φ, it means that the localization axis A forms an angle φ with the z axis. For H$_2$X molecules (see Ref. [33] and references therein) the localization axes were found to coincide essentially with the bonds of the molecule.

For a non-planar molecule, it is more complicated to determine the localization axes. The orientation of a localization axis A relative to the molecule-fixed axis system is given by two standard spherical coordinates θ_A, ϕ_A (i.e., a polar and an azimuthal angle). An approach similar to that described above for H$_2$X molecules was used in Ref. [20] to determine the localization axes for PH$_3$. Only the polar angle θ_A had to be varied; ϕ_A was determined by the fact that for symmetry reasons, the localization axes were found in planes containing the z axis and one P–H bond. Similarly to the case of the H$_2$X molecules, the localization axes in PH$_3$ were found to be close to the P–H bonds [20].

For an XHD$_2$ molecule, we expect to find the localization axes A close to, but not exactly coinciding with, the X–D$_i$ bonds. We cannot, however, eliminate ϕ_A by means of symmetry arguments and have to vary both of the angles (θ_A, ϕ_A) when searching for the localization axis A. We make use of an approach similar to one already presented in Ref. [20]. In the molecule-fixed axis system, the direction of the localization axis A is given by a unit vector $\mathbf{e}_A$ with coordinates

$$(R_x, R_y, R_z) = (\sin\theta_A \cos\phi_A, \sin\theta_A \sin\phi_A, \cos\theta_A) \qquad (6)$$

and the projection of the angular momentum onto the axis A is represented by the operator

$$\mathbf{e}_A \cdot \hat{\mathbf{J}} = R_x \hat{J}_x + R_y \hat{J}_y + R_z \hat{J}_z. \qquad (7)$$

For a primitive cluster state $|j\,\mathrm{PCS}\rangle$, the projection of the angular momentum on the A axis is

$$J_A(\theta_A, \phi_A) = \left\langle j\,\mathrm{PCS} \mid \mathbf{e}_A \cdot \hat{\mathbf{J}} \mid j\,\mathrm{PCS} \right\rangle$$
$$= \sum_{i'',\Gamma''} \sum_{i',\Gamma'} \left(C_{i'',\Gamma''}^{(j)} \right)^* C_{i',\Gamma'}^{(j)} \sum_{\alpha=x,y,z} R_\alpha \left\langle \psi_{i''}^{\Gamma''} \left| \hat{J}_\alpha \right| \psi_{i'}^{\Gamma'} \right\rangle. \qquad (8)$$

A maximum of the functional Eq. (8) $|J_A(\theta_A, \phi_A)| = J\hbar$ defines, to the highest extent allowed by quantum mechanics, a localization axis A. Fig. 6 shows a radial plot of $|J_A(\theta_A, \phi_A)|$ for $J = 60$. We call such a plot an 'angular momentum surface' (AMS), it is a quantum-mechanical analogue of the classical RES. The local maxima of the AMS correspond to the extremal values $-J\hbar$ or $+J\hbar$ of $J_A(\theta_A, \phi_A)$ and so to the desired localization axes A.

The angular uncertainty δ for the determination of the directions A can be estimated as $\arccos[\sqrt{J/(J+1)}]$ [40].

Owing to the definition of our basis functions in Eq. (3), the AMS is unchanged by reflection in the xy plane (see Fig. 6) and it is invariant under the $\mathbf{C}_{2v}(\mathrm{M})$ symmetry operations described above. The AMS consists of eight symmetrically equivalent sections connected by reflections in the xy, xz, and yz planes. Therefore, we can limit the search for extrema to the section with $x \geqslant 0$, $y \geqslant 0$, and $z \geqslant 0$. We use the Newton–Raphson algorithm (see, for example, Ref. [48]) to locate the extrema of $J_A(\theta_A, \phi_A)$ (and thus the localization axes) for $J=40, \ldots, 70$. The azimuthal angle ϕ_A is found close to 90° for all cluster states, while the polar angle θ_A varies from 128.2° for $J = 40$ to 133.1° for $J = 70$. The values of θ_A, determined as described here, are represented by squares in Fig. 7. The 'equilibrium direction' of the vector Bi–D$_1$ in the xyz axis system is defined by (polar, azimuthal) angles of (134.9°, 90.1°). It should be noted that in the present work, we do not obtain the PCS functions $|j\,\mathrm{PCS}\rangle$ by the technique discussed in connection with Eq. (5) above. Instead, we obtain them as eigenfunctions of the operator in Eq. (7) with eigenvalues $\pm J\hbar$. These eigenfunctions are being computed by matrix diagonalization in a basis of ψ_i^{Γ} functions.
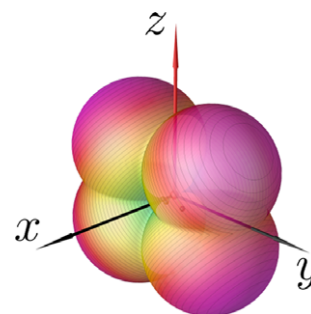

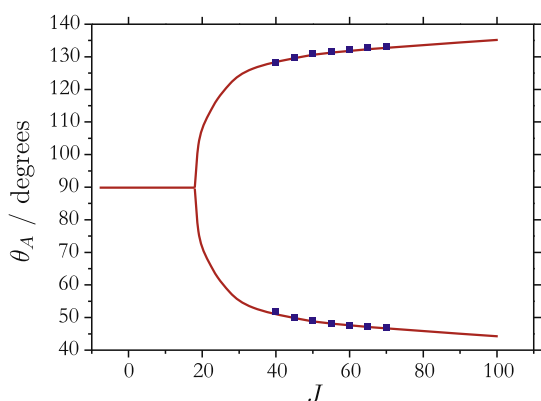**Fig. 6.** The angular momentum surface of BiHD$_2$ at $J = 60$ (see text).

Fig. 7. The polar angle θ_A defining the localization axis A (with $\phi_A = 90°$; see text) for BiHD$_2$. Polar angle values $\theta_A^{(0)}$ obtained by maximizing the function $J_A(\theta_A, \phi_A)$ in Eq. (8) for different values of J are indicated as filled squares. The function $\theta(J)$, indicated as a solid curve, is obtained from semiclassical analysis (see Section 4.1).

For BiHD$_2$, we consider the fourfold rotational clusters to have been formed for $J \geqslant 40$. At $J = 40$, the cluster spread (Fig. 5) is around 10^{-3} cm^{-1}. The procedure described above is explicitly based on the near-degeneracy of the cluster states and, therefore, it cannot be used for $J \leqslant 40$, where there are 'bifurcation effects'. This will be addressed further in the next section where we describe an analysis by means of classical methods.

4. Classical analysis

In the present section, we discuss the mechanisms leading to the energy cluster formation in terms of classical concepts, most notably in terms of the RES [40,41]. We make this analysis for BiH$_2$D and BiHD$_2$ only.

4.1. The rotational energy surface

Harter and Patterson [40,41] have shown that by analyzing the topology of the RES one can explain and predict energy cluster formation. The RES is a radial plot of the function $E_J(\theta, \phi)$ which expresses the classical rotational energy in terms of two angles (θ, ϕ); these angles define the orientation of the classical angular momentum in the molecule-fixed axis system according to the relations

$$J_x = \sqrt{J(J+1)} \sin\theta \cos\phi \tag{9}$$

$$J_y = \sqrt{J(J+1)} \sin\theta \sin\phi \tag{10}$$

$$J_z = \sqrt{J(J+1)} \cos\theta, \tag{11}$$

where $\theta \in [0, \pi]$ and $\phi \in [0, 2\pi]$. In obtaining $E_J(\theta, \phi)$, we replace in the molecular Hamiltonian the angular momentum operators $(\hat{J}_x, \hat{J}_y, \hat{J}_z)$ by their classical analogues in Eqs. (9)–(11) and set the generalized vibrational momenta $p_n = \partial T/\partial \dot{q}_n$ to zero [17]. Here T is the classical kinetic energy and the momentum $p_n, n = 1, 2, \ldots, 6$, is conjugate to the generalized coordinate $q_n \in \{r_1, r_2, r_3, \alpha_{12}, \alpha_{13}, \alpha_{23}\}$ described above. We follow Refs. [20,22] in generating values of $E_J(\theta, \phi)$ on a regular grid of angle points θ_m, ϕ_m. At each such angle point, we minimize the classical energy $E = H_{rv}(r_1, r_2, r_3, \alpha_{12}, \alpha_{13}, \alpha_{23}; \theta_m, \phi_m)$ by optimization of the vibrational coordinates r_i and α_{jk}. The classical rovibrational Hamiltonian function H_{rv} is given by the same kinetic-energy expansion coefficients $G_{\lambda\mu}$, the same pseudo-potential U, and the same potential energy V [42] as used in the variational calculations described in Section 2. That is, the rotational energy surface $E_J(\theta_m, \phi_m)$ is given by

$$E_J(\theta_m, \phi_m) = H_{rv}(J, r_i = r_i^{opt}, \alpha_{jk} = \alpha_{jk}^{opt}; \theta_m, \phi_m), \tag{12}$$

where the classical Hamiltonian function H_{rv} is calculated at the optimized geometries $r_i^{opt}, \alpha_{jk}^{opt}$ for each orientation of the angular momentum defined by the polar and azimuthal angles (θ_m, ϕ_m) and Eqs. (9)–(11). To be able to appreciate better the topology of the RES, we represent it as a radial plot of the function

$$E_J^{(RES)}(\theta_m, \phi_m) = E_J(\theta_m, \phi_m) - E_J^{(min)}, \tag{13}$$

where $E_J^{(min)}$ is the minimum value of $E_J(\theta_m, \phi_m)$. On the RES, we draw 'contour lines' at the variationally computed rotational term values $E_{v=0,J,k}$ (see Fig. 2).

In Fig. 8, we show the RES obtained for BiH$_2$D at $J = 40$. The rotational energies calculated quantum mechanically for this molecule (Fig. 2) show only the twofold cluster formation typical for rigid rotors [47]. Accordingly, the RES exhibits two distinct maxima oriented along the axis characterized by the smallest moment of inertia of the near-prolate top BiH$_2$D. All RESs computed for $J > 0$ have similar topologies and no bifurcation occurs.

By contrast, the RESs constructed for BiHD$_2$ exhibit qualitative changes as J increases. In Fig. 9, we show such RESs computed for $J = 20$, 40, and 80. For $J < 20$, there are no well-defined local maxima, but four such maxima start evolving at $J \geqslant 20$. They define orientations of the classical angular momentum (Eqs. (9)–(11)), and thus of the rotational axes, close to the orientations of the Bi–D bonds. The value of $J = 20$, where the four maxima on the RES emerge, coincides with the value of $J_c = 20$ determined from Fig. 2 (see Section 2). In fact this form of the RES with four maxima was predicted by Harter and Petterson [40] using the semiclassical approach based on the expansion of the rotational
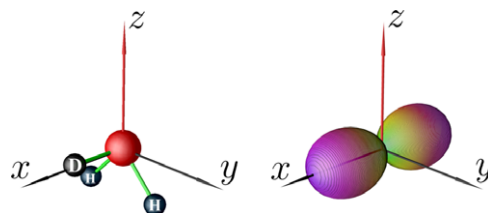

Fig. 8. The rotational energy surface of BiH$_2$D at $J = 40$. The contour lines on the RES represent the (quantum-mechanical) rotational term values $E_{v=0,J,k}$ from Fig. 2.
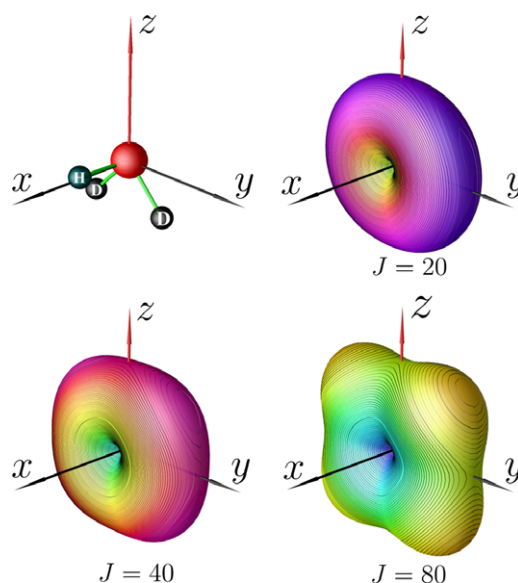

Fig. 9. The rotational energy surfaces of BiHD$_2$ at $J = 20$, 40, and 80. The contour lines on the RESs represent the (quantum-mechanical) rotational term values $E_{v=0,J,k}$ from Fig. 2.

Hamiltonian. Their RES sketched for a hypothetical semirigid asymmetric rotor (Fig. 3 of Ref. [40]) also exhibits a "four-horn" shape very similar to the RESs in Fig. 9.

The stable rotational axes A are classically defined by those directions of the angular momentum that correspond to stationary points on the RES. The RESs in Fig. 9 have four distinct equivalent maxima. These form two pairs with the members of a pair defining classical angular momentum vectors that we can write as $\pm \mathbf{J}$. These two angular momentum vectors describe clockwise and anticlockwise rotation, respectively, about one stable rotational axis, and so the four local maxima define two such axes. For all J values, the stable axes lie close to the yz plane with the azimuthal angle $\phi \approx 90°$. The dependence of the polar angle θ on J exhibits a 'bifurcation' behavior as shown in Fig. 7. In this diagram, we have included the θ-values determined from the RES as solid curves. This diagram unambiguously defines the (classical) critical J-value to be $J_c = 20$. As described in Section 3.2, Fig. 7 also gives the quantum-mechanical θ_A-values obtained by maximizing $|J_A(\theta_A, \phi_A)|$ in Eq. (8) and it is reassuring that these values are in perfect agreement with their classical counterparts.

In Ref. [35], Petrov and Kozlovskii introduced a so-called 'quasi-classical' critical value J_{qc} corresponding to the formation of the first classical trajectory around the local maximum on the RES. We do not repeat their analysis in terms of Bohr–Sommerfeld quantization here, but we estimate from the BiHD$_2$ energy level pattern in Fig. 5 that $J_{qc} \approx 40$ for BiHD$_2$.

According to Eq. (12), each point on the RES of BiHD$_2$ corresponds to an optimized geometry given by, in an obvious notation, values of r_{BiH}^{opt}, $r_{BiD_1}^{opt}$, $r_{BiD_2}^{opt}$, $\alpha_{HBiD_1}^{opt}$, $\alpha_{HBiD_2}^{opt}$, and $\alpha_{D_1BiD_2}^{opt}$. These optimized geometries reflect the dynamical centrifugal effects that accompany the cluster formation [20]. For a clockwise rotation about the Bi–D$_1$ bond, the latter bond stays almost unchanged as J increases, while the bonds Bi–D$_2$ and Bi–H exhibit strong influence of the centrifugal distortion effects, the former being two times larger. At $J = 60$ the Bi–D$_1$, Bi–D$_2$, and Bi–H bonds are found to be elongated by 0.00004, 0.050, and 0.025 Å, respectively. At very high J (> 60), the stationary axes tend to coincide with one of the Bi–D bonds, with the two other bonds being almost perfectly orthogonal to this bond and to each other. As J increases, centrifugal distortion keeps elongating the two bonds orthogonal to the rotation axis until they eventually break.

In addition to these fourfold local maxima the RESs of BiHD$_2$ are characterized by two minima for any $J > 0$ found at $\theta = 90°, \phi = 0°$ and $\theta = 90°, \phi = 180°$, respectively. These minima correspond to the trivial rotations of the rigid symmetric rotor about the c-axis close to the Bi–H bond.

4.2. The θ_k analysis

In the quantum-mechanical TROVE approach [42] the wave-functions are characterized by the quantity $K_{lc} = |k_{lc}|$, where k_{lc} is defined in connection with Eq. (4), it is the value of k for the basis function $\phi_{v,k}^{J,m}$ with the largest contribution to the eigenfunction $\psi_n^{J,\Gamma}$.

Following Refs. [22,40], we introduce the angle θ_k as

$$\theta_k = \arccos\left(\frac{\pm K_{lc}}{\sqrt{J(J+1)}}\right). \tag{14}$$

In the classical limit, θ_k is the angle between the angular momentum vector (and hence the rotation axis) and the z axis. Each eigenfunction $\psi_n^{J\Gamma}$ can be associated with a rotation axis defined by θ_k.

Fig. 10 shows points (θ_k, E_{Jk}) for $J = 60$, where θ_k is calculated from Eq. (14) with K_{lc} taken from the TROVE calculation, which also delivers the value of the rotation–vibration energy E_{Jk}.

Since K_{lc} is the absolute value of the projection of the angular momentum onto the z axis, we cannot determine the sign of
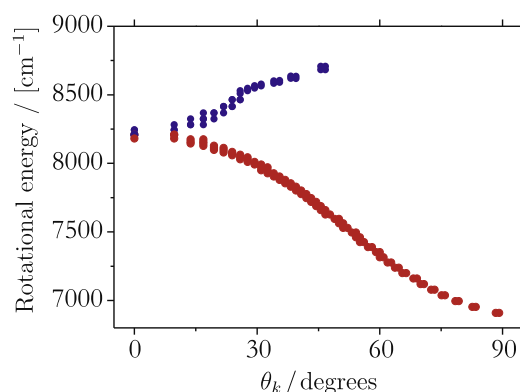

Fig. 10. Energy points (θ_k, E_{Jk}) for the vibrational ground state of BiHD$_2$ at $J = 60$ (see text).
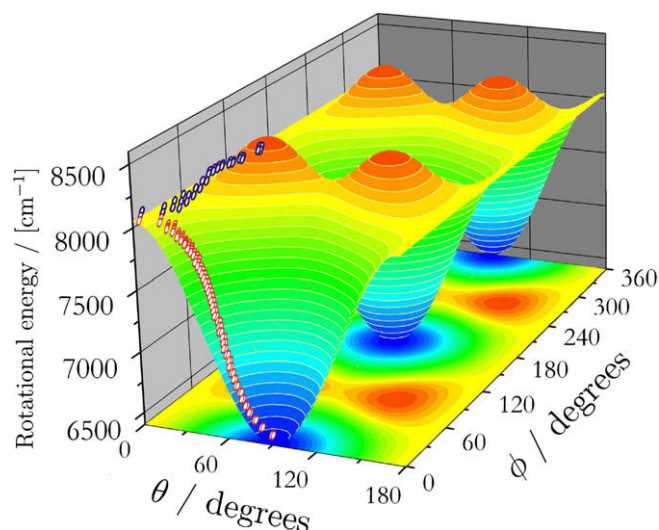

Fig. 11. The rotational energy surface of BiHD$_2$ and the variational energy points (θ_k, E_{Jk}).

$\cos(\theta_k)$. That is, in determining θ_k, we have to choose between $+K_{lc}$ and $-K_{lc}$ in Eq. (14) (see Ref. [22] for details on the points distribution between the 'northern' ($\theta_k < 90°$) or 'southern' ($\theta_k > 90°$) rotational hemisphere).

For comparison, we plot in Fig. 11 the $J = 60$ RES of BiHD$_2$ as a function of (θ, ϕ), and we indicate schematically the steepest-descent path on the RES connecting one of the maxima with one of the minima. This steepest-descent path has a shape very similar to the θ_K curve of Fig. 10. That is, the 'semi-quantum-mechanical' θ_k analysis [22] 'reconstructs' rather accurately the classical RES and demonstrates the correspondence between the quantum-mechanical and classical descriptions.

5. Experimental data

Energy clusters have been experimentally observed chiefly for H$_2$Se [13,23,24], CH$_4$, SiH$_4$ (see [10] and references therein), and SF$_6$ [25].

To our knowledge there has been no experimental verification of energy cluster formation in the spectra of XH$_3$ molecules or their isotopologues. For the XH$_2$D/XHD$_2$ species PH$_2$D/PHD$_2$ [49], the rotational energy level pattern has been experimentally characterized for $J \leqslant 30$, and for AsH$_2$D/AsHD$_2$ [50,51] similar studies have been made for $J \leqslant 21$. Fig. 3 shows that in order to observe cluster formation in PHD$_2$, it is necessary to observe transitions involving

states with $J \approx 60$, which is far beyond the actual experimental possibilities. However indirect evidence for cluster formation can be obtained by extrapolating the experimental rotational energies to high J (see, for example, Ref. [20] for such an extrapolation of the rotational term values of PH$_3$ up to $J = 60$, far above the experimental range of $J \leqslant 23$ [52]). In Fig. 12, we compare the TROVE-calculated PHD$_2$ rotational term values of the present work with values obtained by extrapolation of an effective rotational Hamiltonian with experimentally derived spectroscopic parameter values from Ref. [49]. The calculations with the effective rotational Hamiltonian were carried out with the computer program PGO-PHER [53]. In Fig. 12, the circles show the experimentally derived term values, the solid lines represent the predictions obtained with the effective rotational Hamiltonian, and the short horizontal lines represent the TROVE-calculated values. The theoretical values reproduce well the available experimental results, and at higher J values there is broad agreement between the two theoretical approaches, which both predict energy cluster formation around $J \approx 60$. The larger deviations between the theoretical approaches at J near 70 may be due to lack of convergence of the effective rotational Hamiltonian.

We have not made TROVE calculations for AsH$_2$D and AsHD$_2$ since we have no accurate potential energy surface for AsH$_3$. However, we can make an extrapolation to high J values by means of an effective rotational Hamiltonian as described for PHD$_2$ above; for AsH$_2$D and AsHD$_2$ we use experimentally derived spectroscopic parameter values from Refs. [50,51]. The results of the extrapolation are presented in Fig. 13. Rather surprisingly, we find clusters for AsH$_2$D, but none for AsHD$_2$. This is opposite to our results for the isotopologues of BiH$_3$, PH$_3$, and SbH$_3$ (Figs. 2–4). In AsH$_2$D, the energy clusters appear around $J = 55$, which is far from the experimentally characterized region for this molecule. The 'opposite' findings for, on one hand, the isotopologues of BiH$_3$, PH$_3$, and SbH$_3$ and, on the other hand, the isotopologues of AsH$_3$ show that the reason for the energy cluster formation in pyramidal molecules is not only to be sought in the molecular structure, the cluster formation also depends crucially on the potential energy function of the molecule in question. We intend to extend our quantum-mechanical studies to AsH$_3$, AsH$_2$D, and AsHD$_2$ (by obtaining a potential energy surface more accurate than those presently available) to elucidate also the energy cluster formation in these molecules.

6. Summary and conclusion

To assess the quality of the TROVE calculations reported here, it is important to estimate the convergence of the results, i.e., the adequacy of the basis sets used in the variational calculations. We have used here a relatively small vibrational basis set and focused on rotationally highly excited states. However, we have validated our results by comparing them with term values obtained by extrapolation of experimental results, and we have analyzed the energy level patterns in terms of classical models. Both the comparison with extrapolated experimental term values and the classical analysis lend credibility to the conclusions made from the TROVE results. In addition, for BiHD$_2$ we have performed calculations with a larger basis set defined by $P_{max} = 8$ for rotational excitation up to $J = 60$. The cluster formation diagram obtained with this basis set is highly similar to that in Fig. 2 and so the cluster formation appears to be well described by the $P_{max} = 6$ basis set.

In conclusion, we have reported here theoretical evidence for the formation of clusters in the energy spectra of XHD$_2$ molecules. The evidence is chiefly based on variational calculations, using the program TROVE [42], of the rotational energy level patterns of BiHD$_2$, PHD$_2$, and SbHD$_2$. We have shown that for X = P, Bi, and Sb, the isotopologue XHD$_2$ exhibits fourfold energy clusters at high rotational excitation, whereas the isotopologue XH$_2$D does not. We have further demonstrated this result to be in accordance with classical analysis in terms of the RES.

Among the XH$_3$ molecules studied previously [20,22], the most pronounced energy cluster formation was found for BiH$_3$. Similarly, the quantum-mechanical studies of the present work predict the most pronounced energy cluster formation for BiHD$_2$. This can be traced to the strong local-mode character of this molecule as
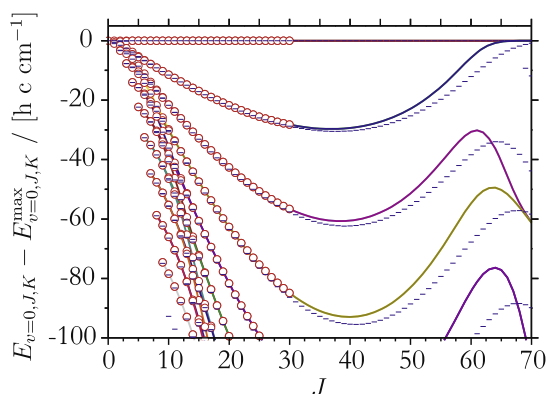

Fig. 12. Calculated rotational energy levels of PH$_2$D in the ground vibrational state plotted relative to the highest term for each J multiplet. Circles represent the experimentally derived term values. Variationally calculated term values are drawn as short horizontal lines. Solid curves represent the eigenvalues of an effective rotational Hamiltonian with parameters obtained by fitting to experimental data [52]. From top to bottom, successive curves correlate with rigid-rotor states having increasing values of $|k_c| = 0, 1, 2, \ldots$.
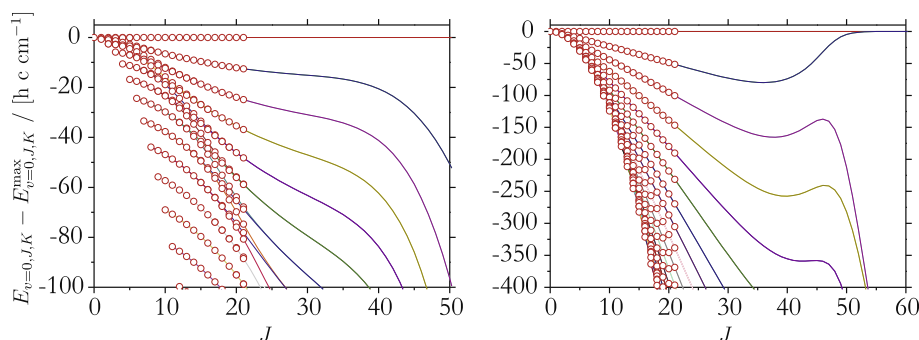

Fig. 13. Extrapolated rotational energy levels of AsHD$_2$ (left) and AsH$_2$D (right) in the ground vibrational state plotted relative to the highest term for each J multiplet: circles represent the experimentally derived term values and solid curves represent the eigenvalues of an effective rotational Hamiltonian with parameters obtained by fitting to experimental data [50,51].

compared to PHD$_2$ and SbHD$_2$ [22]. While XH$_3$ molecules have six-fold energy clusters, the XHD$_2$ molecules exhibit fourfold clusters very similar to those of H$_2$X species. As usual, the classical motion of the XHD$_2$ molecule can be thought of as a rotation about one of the X–D bonds. Centrifugal forces are mostly responsible for forming these rotation energy clusters.

We find that at high J, there are stable rotations about all the three bonds X–H, X–D$_1$, and X–D$_2$ in XHD$_2$ molecules with X = Bi, P, and Sb, but the X–H and X–D rotations are energetically well separated from each other and from the vibration modes. The two rotational axes X–D$_i$ are equivalent, similar to the H$_2$X case. As already mentioned, the isotopologues XH$_2$D (with X = Bi, P, and Sb) do not exhibit energy cluster formation. In order that clusters can form at the top of the J-manifolds, it must be possible for the molecule to have multiple equivalent, localized rotational axes associated with small values of the moment of inertia (i.e., with large values of the rotational constant). For the near-oblate XHD$_2$ molecules this condition is more easily satisfied than in the near-prolate XH$_2$D molecules (see the approximate location of the *abc* axes in Fig. 1). Thus, the equivalent X–H bonds in the XH$_2$D species cannot provide stability for rotation in the same way as the X–D bonds in the XHD$_2$ species can.

Acknowledgments

References

[1] A.J. Dorney, J.K.G. Watson, J. Mol. Spectrosc. 42 (1972) 135–148.
[2] K. Fox, H.W. Galbraith, B.J. Krohn, J.D. Louck, Phys. Rev. A15 (1977) 1363–1381.
[3] W.G. Harter, C.W. Patterson, Phys. Rev. Lett. 38 (1977) 224–227.
[4] W.G. Harter, C.W. Patterson, J. Chem. Phys. 66 (1977) 4866–4885.
[5] W.G. Harter, C.W. Patterson, J. Chem. Phys. 66 (1977) 4886–4892.
[6] W.G. Harter, C.W. Patterson, F.J. da Paixao, Rev. Mod. Phys. 50 (1978) 37–83.
[7] B.I. Zhilinskiy, I.M. Pavlichenkov, Opt. Spectrosc. (USSR) 64 (1988) 688–690.
[8] J. Makarewicz, J. Pyka, Mol. Phys. 68 (1989) 107–127.
[9] J. Makarewicz, Mol. Phys. 69 (1990) 903–921.
[10] D.A. Sadovskii, B.I. Zhilinskii, J.P. Champion, G. Pierre, J. Chem. Phys. 92 (1990) 1523–1537.
[11] J. Pyka, Mol. Phys. 70 (1990) 547–561.
[12] K.K. Lehmann, J. Chem. Phys. 95 (1991) 2361–2370.
[13] I.N. Kozin, S. Klee, P. Jensen, O.L. Polyansky, I.M. Pavlichenkov, J. Mol. Spectrosc. 158 (1993) 409–422.
[14] P. Jensen, I.N. Kozin, J. Mol. Spectrosc. 160 (1993) 39–57.
[15] I.N. Kozin, P. Jensen, J. Mol. Spectrosc. 161 (1993) 186–207.
[16] S. Brodersen, B.I. Zhilinskii, J. Mol. Spectrosc. 172 (1995) 303–318.
[17] I.N. Kozin, I.M. Pavlichenkov, J. Chem. Phys. 104 (1996) 4105–4113.
[18] P.C. Gómez, P. Jensen, J. Mol. Spectrosc. 185 (1997) 282–289.
[19] P. Jensen, Mol. Phys. 98 (2000) 1253–1285.
[20] S.N. Yurchenko, W. Thiel, S. Patchkovskii, P. Jensen, Phys. Chem. Chem. Phys. 7 (2005) 573–582.
[21] S.N. Yurchenko, M. Carvajal, W. Thiel, P. Jensen, J. Mol. Spectrosc. 239 (2006) 71–87.
[22] S.N. Yurchenko, W. Thiel, P. Jensen, J. Mol. Spectrosc. 240 (2006) 174–187.
[23] I.N. Kozin, S.P. Belov, O.L. Polyansky, M. Yu. Tretyakov, J. Mol. Spectrosc. 152 (1992) 13–28.
[24] I.N. Kozin, O.L. Polyanski, S.I. Pripolzin, V.L. Vaks, J. Mol. Spectrosc. 156 (1992) 504–506.
[25] J.P. Aldridge, H. Filip, H. Flicker, R.F. Holland, R.S. McDowell, N.G. Nereson, K. Fox, J. Mol. Spectrosc. 58 (1975) 165–168.
[26] S.N. Yurchenko, M. Carvajal, P. Jensen, H. Lin, J.J. Zheng, W. Thiel, Mol. Phys. 103 (2005) 359–378.
[27] S.N. Yurchenko, M. Carvajal, W. Thiel, H. Lin, P. Jensen, Adv. Quant. Chem. 48 (2005) 209–238.
[28] J.T. Hougen, P.R. Bunker, J.W.C. Johns, J. Mol. Spectrosc. 34 (1970) 136–172.
[29] C. Eckart, Phys. Rev. 47 (1935) 552–558.
[30] A. Sayvetz, J. Chem. Phys. 7 (1939) 383–389.
[31] R.I. Ovsyannikov, W. Thiel, S.N. Yurchenko, M. Carvajal, P. Jensen, J. Mol. Spectrosc. 252 (2008) 121–128.
[32] S.N. Yurchenko, M. Carvajal, H. Lin, J.J. Zheng, W. Thiel, P. Jensen, J. Chem. Phys. 122 (2005) 104317.
[33] P. Jensen, G. Osmann, I.N. Kozin, in: D. Papoušek (Ed.), Vibration-Rotational Spectroscopy and Molecular Dynamics, World Scientific, Singapore, 1997.
[34] P. Jensen, I.N. Kozin, J. Mol. Spectrosc. 163 (1994) 483–509.
[35] S.V. Petrov, B.M. Kozlovskii, J. Mol. Spectrosc. 243 (2007) 245–252.
[36] S.M. Colwell, N.C. Handy, W.H. Miller, J. Chem. Phys. 68 (1978) 745–749.
[37] W.G. Harter, C.W. Patterson, Phys. Rev. A 19 (1979) 2277–2303.
[38] W.G. Harter, C.W. Patterson, J. Math. Phys. 20 (1979) 1453–1459.
[39] W.G. Harter, Phys. Rev. A 24 (1981) 192–263.
[40] W.G. Harter, C.W. Patterson, J. Chem. Phys. 80 (1984) 4241–4261.
[41] W.G. Harter, Comp. Phys. Rep. 8 (1988) 319–394.
[42] S.N. Yurchenko, W. Thiel, P. Jensen, J. Mol. Spectrosc. 245 (2007) 126–140.
[43] M.S. Child, L. Halonen, Adv. Chem. Phys. 57 (1984) 1–58.
[44] L. Halonen, A.G. Robiette, J. Chem. Phys 84 (1986) 6861–6871.
[45] W. Jerzembeck, H. Bürger, L. Constantin, L. Margulès, J. Demaison, J. Breidung, W. Thiel, Angew. Chem. Int. Ed. 41 (2002) 2550–2552.
[46] P.R. Bunker, P. Jensen, Molecular Symmetry and Spectroscopy, second ed., NRC Research Press, Ottawa, 1998.
[47] D. Papoušek, M.R. Aliev, Molecular Vibrational–Rotational Spectra, Elsevier, Amsterdam, 1982.
[48] J.M. Thijssen, Computational Physics, Cambridge University Press, Cambridge, 1999.
[49] O.N. Ulenikov, H. Bürger, W. Jerzembeck, G.A. Onopenko, E.S. Bekhtereva, O.L. Petrunina, J. Mol. Struct. (THEOCHEM) 599 (2001) 225–237.
[50] O.N. Ulenikov, E.S. Bekhtereva, A.S. Bulavenkova, C. Leroy, W. Jerzembeck, H. Bürger, J. Mol. Spectrosc. 240 (2006) 102–111.
[51] O.N. Ulenikov, E.S. Bekhtereva, O.V. Gromova, T.D. Chudinova, W. Jerzembeck, H. Bürger, J. Mol. Spectrosc. 251 (2008) 114–122.
[52] L. Fusina, G. Di Lonardo, J. Mol. Struct. (THEOCHEM) 517–518 (2000) 67–78.
[53] PGOPHER, a Program for Simulating Rotational Structure, C.M. Western, University of Bristol. Available from: <http://pgopher.chm.bris.ac.uk>.